### Title
A new second-order numerical manifold method model with an efficient scheme for analyzing free surface flow with inner drains




### Journal
Applied Mathematical Modelling, 40(2)

### ISSN
0307-904X



### Authors
Wang, Yuan
Hu, Mengsu
Zhou, Quanlin
et al.



### Publication Date
2016

### DOI
10.1016/j.apm.2015.08.002

Peer reviewed

# A new second-order numerical manifold method model with an efficient scheme for analyzing free surface flow with inner drains

Yuan Wang[a,b,*], Mengsu Hu[a,b], Quanlin Zhou[b], Jonny Rutqvist[b]

[a] College of Civil and Transportation Engineering, Hohai University, Nanjing 210098, China

[b] Earth Sciences Division, Lawrence Berkeley National Laboratory, Berkeley, CA 94720, USA

a r t i c l e i n f o

*Keywords:*
Numerical manifold method
Second-order
Free surface flow
Inner drain Fixed
mesh
Flux calculation

a b s t r a c t

Numerical manifold method (NMM) is a numerical method known for analyzing continuous and discontinuous mechanical processes in a unified mathematical form. In this study we developed a new second-order NMM model to solve the nonlinear problem of water flow with the free surface priori unknown and the difficulty of modeling drains which could dramatically increase the meshing load. Our study consist of: (1) deriving two forms of NMM second-order approximation; (2) constructing the total potential energy for water flow by our energy-work seepage model considering Dirichlet, Neumann and material boundaries uniformly; (3) locat- ing free surface nodes in two forms of second-order approximation; (4) tracking the free sur- face with an efficient iteration scheme without re-meshing; (5) deriving velocity and tunnel flux by second-order approximation. We developed a new code and demonstrate our model and code with examples including confined drainage tunnel and free surface flow through a dam. We compare the results such as tunnel flux or free surface with linear NMM, analytical or other available numerical solutions. We prove that: the two forms of second-order NMM (1) yield consistent results; (2) for modeling drains involving local intensive change, could achieve accurate result of tunnel flux calculation and dramatically save computation load with linear velocity distribution in coarse mesh; (3) for free surface iteration, are efficient with fast con- vergence to accurate results and with rather coarse mesh. As a result, our second-order NMM model is applicable to free surface flow with inner drains for free surface locating and flux calculation, and seepage stability analysis, laying a solid foundation for extending to coupled hydro-mechanical analysis.



## 1. Introduction

Numerical modeling of groundwater flow in unconfined aquifers are of great interest and concerns to groundwater hydrologists [1–4]. It is often conducted to simulate natural recharge or discharge, and well pumping or injection and assess their effects on groundwater systems at a large scale (up to hundreds of kilometers). For flow in geotechnical and hydraulic engineering at a smaller scale (from 10 to 1000 m), analysis of free surface (unconfined) flow is also important and is often used to predict tunnel inflow and the associated safety or environmental impacts [5,6] or to assess potential seepage instability (e.g. erosion, piping, hydraulic fracturing) in embankment dams [7–9]. At both scales, the free surface flow consists of unsaturated and underlying

* Corresponding author. Tel.: +86 13951002717.
*E-mail address:* wangyuanhhu@163.com (Y. Wang).

http://dx.doi.org/10.1016/j.apm.2015.08.002
S0307-904X(15)00445-X/

**Notations**

| | |
|---|---|
| h | hydraulic head |
| hi(x, y) hj | the hydraulic head on physical cover i |
| nx and ny | the jth degree of freedom of physical cover i |
| qi qn | the cosine of the normal vector of the boundary relative to the horizontal and vertical directions, respectively. water pressure |
| q¯x and q¯y | flux through each pipe |
| r s sj **v** | the normal flux across a boundary the known flux components |
| wi(x, y) y | the total number of physical covers for the model domain the length of each pipe |
| Cij Hi **K** | the coefficient of freedom |
| Npc(e) | the Darcy flow velocity vector |
| Q i | the weight function on physical cover i related to element e |
| Ui Wg | the vertical direction |
| Wm Wp Ws Wv | the component the given hydraulic head |
| γ | the tensor matrix of permeability coefficient |
| ζ 1'hp 1'hd | the number of physical covers related to element e |
| ITm ITN | the flux term |
| i | the geometric range of physical cover i |
| | the work by fluid gravity |
| | the work done by fluid flow through material boundaries the work done by water flow |
| | the domain seepage work |
| | the work done by water flow through Dirichlet boundaries the work done by fluid flow through Neumann boundaries the unit weight of water |
| | the coefficient of the linear relationship between qi and 1'hi |
| | hydraulic head difference between the two ends of each pipe |
| | hydraulic head difference across the boundary domain in the pipe flow direction potential energy associated with domain flow work |
| | potential energy associated with gravity work |
| | potential energy associated with flow work for Dirichlet boundary conditions potential energy associated with flow work for material boundaries |
| | potential energy associated with flow work for Neumann boundary conditions a section normal to the i direction |

saturated flow separated by a capillary fringe [1–2]. When the soil parameters (such as water-retention curves) are available, this problem could be solved with the variably-saturated flow formulations by formulating the flow equations in both saturated and unsaturated zones. Such a formulation has been developed by many authors [10–13] and extended to the development and application of coupled flow-mechanical analysis. When the vertical flow is negligible compared with lateral flow and the capil- lary fringe zone is very thin, the capillary fringe can be approximated by a free surface, as a discontinuity in the saturated zone. Solving the moving free surface involves high geometrical nonlinearity but does not involve material nonlinearity in the form of complex water-retention curves required in variably-saturated flow formulations. Different types of free surface formulations exists in other engineering disciplines such as in metal processing [14] and channel and river flow engineering [15–17]. However, the free surface of our interest in this study is different from that in metal processing [14] or fluid dynamics calculated by vol- ume of fluid (VOF), smoothed particle hydrodynamics (SPH), or developed finite volume method (FVM) used in free surface flow [15–17]. In this study, we focus on the free surface flow through porous media in engineering, involving localized flow associated with drains or tunnels, though our model can be applied to large-scale analysis. The basic differences between these two types of free surface flow are: (1) the govern equation used in the hydrodynamics is Navier–Stokes, whereas in engineered problems of our focus could be easily simplified as Darcy's law; (2) in small-scale analysis such as free surface flow in dams, the exact location of the free surface is very key for predicting the stability of the dam especially with high gradient, which sometimes could not be perfectly achieved if without proper surface-locating scheme.

The challenge of free surface flow analysis is to accurately and efficiently locate the free surface, which is unknown a priori. A number of numerical methods have been developed for modeling water flow with a free surface and they can be classified into adaptive-mesh methods and fixed mesh methods. Generally, the adaptive-mesh methods require modifications of the computa- tional mesh for updating the geometry of the simulation domain bounded by the free surface. The mesh is updated through an

iterative process until the change in the free surface position between successive iterations is negligible. A wide range of numer- ical methods have been used with adaptive-mesh methods, including finite difference [18], finite element [4,19,20], boundary element [21], finite volume [22,23], and natural element [24] methods. For the fixed-mesh methods, models with finite element [25–34], finite difference [35], element-free [36], and numerical manifold [37–39] methods have also been developed. In these fixed-mesh methods, the geometrical nonlinearity is solved by (1) being transformed to equivalent nodal flux at each iteration using residual flow [24,25], initial flow [26], etc; or (2) being converted to nodal forces based on the concepts of extended pres- sure defined in a variational inequality formulation [27–29]; or (3) being replaced with a nonlinear constitutive relationship between pore pressure and permeability coefficient across the simulated domain divided by the free surface [30]. In addition to the precision of solutions, the computational cost related to meshing and iterations are key factors in practical applications of these numerical methods.

The challenge of modeling drains or drainage tunnels is to precisely capture the local intense change in hydraulic head and flux around the drains, with complex geometric features (including the location, the orientation, the shape and the size) and boundaries. Both implicit models and explicit models have been developed to avoid relatively time-consuming meshing around the tunnels, especially when a large number of tunnels are involved. In the implicit models, a drainage hole or tunnel is treated as an equivalent discontinuity and its permeability is determined by the equivalent principle of flow rate, related to the rock conductivity and geometric features (the size, orientation and spacing) of the tunnel. In explicit models, a hole or tunnel is treated by substructure techniques, semi-analytical approaches [40], the point well model or the composite element method [41]. By comparison, the implicit models are more capable if a large quantity of holes or tunnels are contained in a medium, whereas the explicit models has the better potential to give more precise solution for describing flow around the tunnels in more details.

The numerical manifold method (NMM) is a promising numerical method for modeling continuous and discontinuous problems proposed by Shi [42–43]. It is based on a finite cover system with independent mathematical and physical covers. The mathematical covers are chosen by users, consist of finite overlapping covers that occupy the entire material domain. Conventional meshes such as regular finite difference grids, finite elements, or convergence regions of series can be used as mathematical covers. These mathematical covers define numerical precision by their density. The physical covers are divided by boundaries or joints from mathematical covers, determining the integration fields. The global behavior can be computed by functions defined in local physical covers. Based on finite covers, the NMM is flexible and general enough to include and combine well-developed analytical methods, the widely-used FEM, and the block-oriented discontinuous deformation analysis (DDA, [44]) in a unified form. Previously, the NMM has been successfully applied to both continuous and discontinuous mechanical analysis [45], including three dimensional discontinuous dynamic analysis [46]. For fluid flow modeling, it was developed and applied in analysis of free surface flow [37–39] and groundwater flow in heterogeneous media [47]. Relevant to analysis of free surface flow possibly with inner drains, the following features of the NMM can be highlighted:

(1) Using NMM with two-mesh system, it is very convenient to handle the discontinuity at the free surface by fixing the mathematical covers and iteratively updating the physical covers to account for the effective contributions from the flow domain. This benefit has been demonstrated in our previous work using the first-order (linear) approximation [38] and the accuracy has been verified.
(2) When applied to cases with inner drains involving intense local changes, the computation precision can be easily enhanced by increasing the approximation order. In NMM, the global approximation field is not defined by a nodal weighted average as in standard FEM, but by the weighted average of cover functions, which could be spatially constant, linear, or an arbitrary user-defined function. The first-order NMM resulting in an element-wise constant velocity field requires refinement of the numerical grid, analogous to common grid refinements in FEM [48]. However, grid- refinement could sometimes be very computationally expensive, when moving boundaries are involved. Alternatively, increasing the order of approximation is an effective way to improve numerical precision, which in NMM is a natural extension of the first-order NMM by increasing the order of either the weight functions or the physical cover functions. For modeling mechanical processes, the efficiency and accuracy of higher-order NMM approximations for regions of high stress and strain gradients have been demonstrated [49–50]. Mathematically, similar advantages of higher-order interpolation should also apply for modeling water flow in porous media involving high hydraulic potential gradients and localized flow.
(3) The simplex integration used in NMM enables deriving analytical solutions for higher-order approximation involving arbitrarily shaped elements [43].
(4) With the fixed mathematical covers used in NMM, the meshing effort can be substantially reduced, especially in the case of moving boundaries [42].

In this study, we developed two forms of second-order NMM model for free surface flow in porous geological media, where an inner drain may be contained. We used the mathematical seepage model through energy-work analysis developed in our previous work [38], with each term providing sound physical meaning for the widely-used variational principle. An algorithm including both forms of the second-order interpolation and an iteration scheme were developed to track the free surface. The velocity and the flux for drainage tunnels were also calculated with both forms. Finally our new second-order NMM model was coded in a computer code package. We applied the computer code to water flow examples involving flow with a priori unknown free surface and problems involving inner drains, and compared our results to those of a first-order NMM model and other available numerical solutions. We showed that the second-order NMM achieves accurate results at a higher convergence speed with relatively coarser numerical grids, demonstrating excellent numerical efficiency.

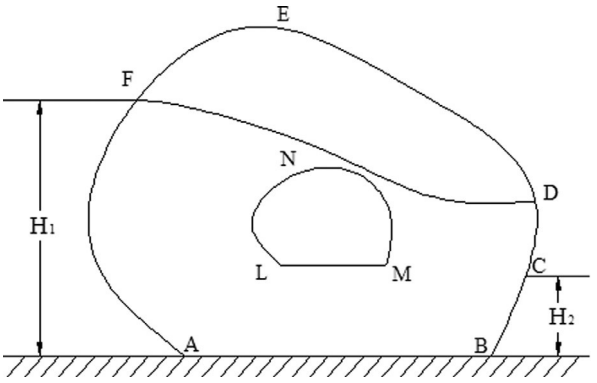


**Fig. 1.** A typical unconfined seepage problem with complex boundaries and an inner tunnel.

As the extension of our previous work using the first-order (linear) approximation [38], the second-order NMM model developed in this study makes the following advancements: (1) the two forms of second-order NMM developed in this study could be reduced to first-order approximation [38] for simplified cases. Therefore, these two forms of second-order approximation will be a mathematical advancement from the first- order work; (2) second-order approximation enables the solution of high-velocity flow problems involving inner drains that could not be readily done using linearly approximated methods (including linear FEM and NMM). With linearly distributed flux, it is superior to linear approximation with constant flux distribution for solving high-gradient and localized flow problems; (3) for the nonlinear and discontinuous problems associated with a free surface, second-order NMM is expected to achieve higher accuracy and convergence rate, which will be verified through demonstration examples.

## 2. Development of second-order NMM model for free surface flow analysis

We developed a second-order NMM model for water flow analysis with a prori-unknown free surface and derived flux calculation for cases involving inner drains. This model consists of a mathematical mesh, which is fixed during the simulation, and a physical mesh, which is divided from the mathematical mesh by domain boundaries (in Section **2.1**) and the free surface (i.e., a discontinuity) and updated iteratively by a developed iteration scheme (**2.4**). The second-order approximation is achieved (**2.2**) using linear physical cover functions with linear weight functions (Form 1) or second-order weight functions with constant cover functions (Form 2). With both forms, we calculated hydraulic head and velocity and flux for drainage tunnels (**2.5**). The equilibrium equations in this NMM model are assembled by the total potential energy, derived through our energy-work seepage model (**2.3**).

### *2.1. Fundamentals of NMM for water flow analysis*

A typical free surface flow through a two-dimensional domain, as shown in Fig. 1, follows the mass conservation

$$\frac{\partial v_x}{\partial x} + \frac{\partial v_y}{\partial y} = 0 \tag{1}$$

and the Darcy's law

$$v_x = -k_{xx}\left(\frac{\partial h}{\partial x}\right) - k_{xy}\left(\frac{\partial h}{\partial y}\right), \quad v_y = -k_{yx}\left(\frac{\partial h}{\partial x}\right) - k_{yy}\left(\frac{\partial h}{\partial y}\right) \quad \text{or} \quad \mathbf{v} = -\mathbf{K}\,\mathbf{grad}(h) \tag{2}$$

where $h$ is the hydraulic head, the sum of elevation $y$ and the pressure head $p/\gamma$, expressed as

$$h = y + \frac{p}{\gamma} \tag{3}$$

**grad**($h$), **v** and **K** are the hydraulic gradient vector, the Darcy flow velocity vector, and the tensor of permeability coefficient. The boundaries consist of: (1) Dirichlet boundaries (such as AF and BC), (2) Neumann boundaries (such as AB), (3) Cauchy boundaries (such as DF, the free surface for this problem), or (4) boundaries such as release surface (CD), and (5) the material boundaries (such as LMN), satisfying

$$h = H_i \tag{4}$$

$$q_n = \_q_x n_x + \_q_y n_y \tag{5}$$

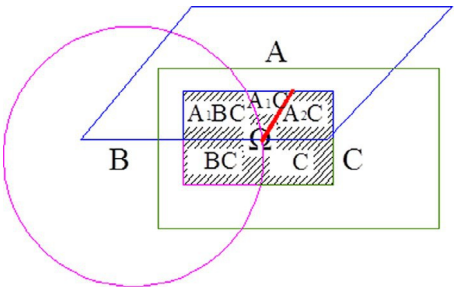


**Fig. 2.** Mathematical covers, physical covers and elements defined in NMM.

$$p = 0 \text{ and } q_n = 0 \tag{6}$$

$$p = 0 \text{ and } q_n < 0 \tag{7}$$

$$h^-_n = h^+_n \text{ and } q^-_n = q^+_n \tag{8}$$

where $H_i$ is the fixed hydraulic head, $q_n$ is the normal flux across a boundary, $q^-_x$ and $q^-_y$ are the given flux components, $n_x$ and $n_y$ are the cosine of the normal vector of the boundary relative to the horizontal and vertical directions, – and + are the negative and positive directions of the normal vector of a boundary respectively.

The boundary LMN is not limited to a material boundary, but could represent a variety of conditions, including the boundary of

(1) a drainage tunnel, satisfying Eq. (4), or
(2) a water tight non-drainage tunnel, satisfying Eq. (5), or
(3) a different material domain, satisfying Eq. (8).

In such a system, the porous media may consist of different materials with different hydraulic properties or contain fractures or holes; the hydraulic gradient could be arbitrarily high, especially around a tunnel; and boundary conditions could be (1) fixed as confined flow, or (2) unknown a priori as a water table in free surface flow, making it nonlinear with the key issue to locate the free surface with a certain iteration scheme.

To represent the complicated model boundaries and track the a priori unknown free surface shown in Fig. 1, we develop a second-order NMM model. Here we briefly describe the fundamental of NMM, including mathematical cover, physical cover, elements, cover functions, and weight functions. We use a general example shown in Fig. 2, with the model domain represented by the shaded part and an inner discontinuity (bold red line). We define three geometric shapes (i.e., mathematical covers) to cover the model domain: the quadrilateral cover A, the circular cover B, and the rectangular cover C, which define interpolation precision. The corresponding physical cover is divided from the mathematical cover by domain boundaries and/or the inner discontinuity. For example, physical cover C is the entire model domain, while physical cover B is divided from mathematical cover B by boundaries. Physical cover A (divided from mathematical cover A by boundaries) is further divided into physical covers $A_1$ and $A_2$ by the inner discontinuity. The overlapping areas by multiple physical covers are defined as elements. As a result, the model domain is discretized into five elements: $A_1BC$ (the intersection of physical cover $A_1$, B and C), $A_1C$, $A_2C$, BC, and C (covered by physical cover C solely). Note the difference between mathematical cover C, physical cover C, and element C.

From Fig. 2, we can see that the shape of the mathematical covers could be arbitrary; the relative location of the mathematical covers to the model domain could also be arbitrary, only if satisfying:

$$\subset A \cup B \cup C \tag{9}$$

and the number of physical covers on each element could be arbitrary. For the uniformity and simplicity of computation, we choose triangles for the mathematical mesh, and this will be described in details in the next two subsections.

The hydraulic head at a point $(x, y)$ in element $e$ is the weighted average of hydraulic head functions of all physical covers overlapping the element:

$$\quad \tag{10}$$

where $N_{pc}$ is the number of physical covers overlapping element $e$, $\{h_i(x, y)\}$ is the hydraulic head function of physical cover $i$, and $w_i(x, y)$ is the weight function of physical cover $i$. For an individual physical cover $i$, we have

$$w_i(x, y) > 0 \ (x, y) \in \quad U_i \quad U_i \tag{11}$$

where $U_i$ is the geometric range of physical cover $i$.

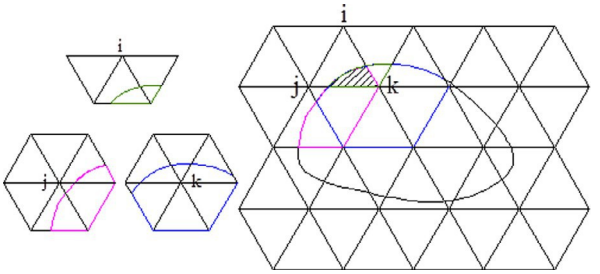


**Fig. 3.** Elements defined in Form 1 second-order interpolation.

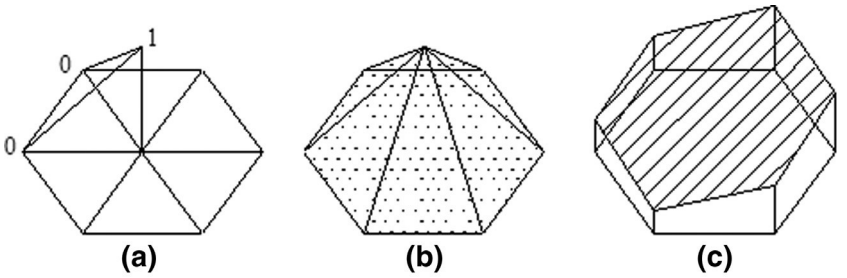


**Fig. 4.** (a), (b) Piecewise linear weight function on a physical cover; (c) Linear hydraulic head on a physical cover.

The hydraulic head function $\{h_i(x, y)\}$ (i.e., cover function) of physical cover $i$ can be a series of any order:

$$h_i(x, y) = \sum_{j=1}^{m} s_j h_{ij} = (1\ x\ y\ \cdots\ s_m) \begin{pmatrix} h_{i1} \\ h_{i2} \\ \vdots \\ h_{im} \end{pmatrix} \tag{12}$$

where $m$ and $h_{ij}$ are the number of degrees of freedom and the $j$th degree of freedom of physical cover $i$, respectively, and $s_j$ is the coefficient of the $j$th degree of freedom. For 2-D flow analysis, $m$ is 1 or 3 when the hydraulic head is 0-order (constant), or first-order. For a complete N-order physical cover function, $m = (N+1)(N+2)/2$. The global approximation on the entire domain is the summation of the contribution of each physical cover to all corresponding elements.

### 2.2. Second-order NMM approximation for water flow simulation

As defined in Section 2.1, the global approximation is the weighted average of local physical cover functions, thus the second-order interpolation could be realized by (1) a linear hydraulic head distribution on a physical cover and a linear weight function (Form 1) or (2) a constant hydraulic head on a physical cover and a second-order weight function (Form 2).

#### 2.2.1. Form 1

The first form of second-order interpolation is illustrated in Fig. 3. For a mathematical mesh system with uniform triangles, all the triangles sharing a certain triangle vertex (such as mathematical covers $i$, $j$ and $k$) form a mathematical cover (i.e., a hexagon). The definition of physical covers and elements follows the same rule as mentioned above. Hence an element is the overlap of three physical covers, such as the shaded part in Fig. 3 overlapped by physical covers $i$, $j$ and $k$.

Fig. 4 shows the second-order interpolation in the form of piecewise linear weight functions, equivalent to the shape functions for triangular elements in FEM expressed as

$$\begin{pmatrix} w_i(x, y) \\ w_j(x, y) \\ w_k(x, y) \end{pmatrix} = (1\ x\ y) \begin{pmatrix} 1 & x_i & y_i \\ 1 & x_j & y_j \\ 1 & x_k & y_k \end{pmatrix}^{-1} \tag{13}$$

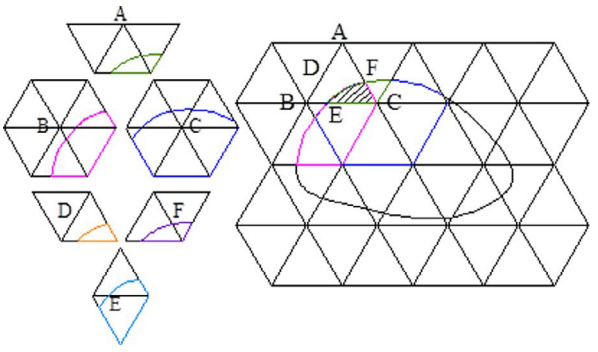


**Fig. 5.** Elements defined in Form 2 second-order interpolation.

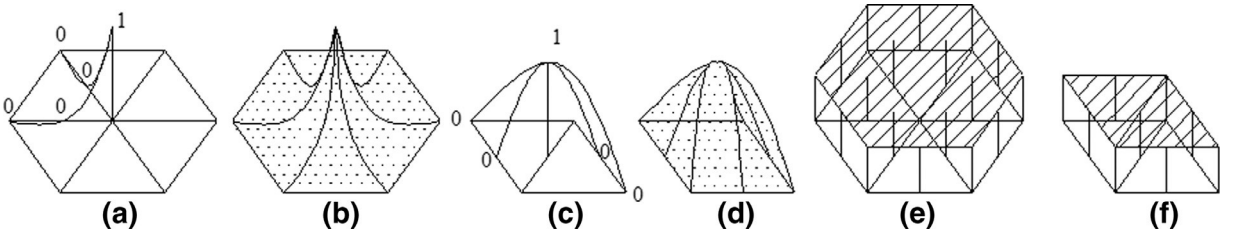


**Fig. 6.** (a), (b) second-order weight function on a physical cover at a vertex; (c), (d) second-order weight function on a physical cover centered at midpoint; (e), (f) constant hydraulic head on a physical cover.

and linearly distributed hydraulic head on a physical cover, which is represented as:

$$h_i(x, y) = (1\ x\ y)\begin{pmatrix} h_{i1} \\ h \\ \end{pmatrix}$$

where $h_{i1}$,$h_{i2}$ and $h_{i3}$ are the three degrees of freedom on a physical cover to be solved. (14)

*2.2.2. Form 2*

In Form 2 of second-order NMM, the shape function is second-order and the hydraulic head is constant on a physical cover. We can accomplish this by changing the mesh shapes, such as using rectangles to form the mathematical covers or by increasing the number of physical covers on each element. In our calculations, we use a six-physical-cover system to form elements, i.e. the physical covers centered at the three vertices of a triangle and at the three midpoints of each edge of the triangle, as covers A, B, C, D, E and F shown in Fig. 5.

Fig. 6(a)–(d) show the second-order weight functions; and (e), (f) show the constant hydraulic head within a physical cover centered at a triangular vertex and midpoint, respectively.

Similar to six-node FEM, the weight functions are:

$$\{w_1\ w_2\ w_3\ w_4\ w_5\ w_6\} = (1\ x\ y\ x^2\ xy\ y^2)\begin{pmatrix} 1 & x_1 & y_1 & x_1^2 & x_1y_1 & y_1^2 \\ 1 & x_2 & y_2 & x_2^2 & x_2y_2 & y_2^2 \\ 1 & x_3 & y_3 & x_3^2 & x_3y_3 & y_3^2 \\ 1 & x_4 & y_4 & x_4^2 & x_4y_4 & y_4^2 \\ 1 & x_5 & y_5 & x_5^2 & x_5y_5 & y_5^2 \\ 1 & x_6 & y_6 & x_6^2 & x_6y_6 & y_6^2 \end{pmatrix}^{-1} \quad (15)$$

and the hydraulic head on physical cover $i$ is:

$$h_i(x, y) = h_i \quad (16)$$

where $h_i$ is the unknown to be solved.

### 2.3. Energy-work seepage model and establishment of equilibrium equations

From mass conservation expressed as Eq. (1) combined with the finite cover approximation as Eqs. (10)–(12), how to set up equilibrium equations is the basic issue for a numerical approximation. Furthermore, there are several issues to be considered when modeling boundaries since it is unnecessary to adjust element nodes to boundaries in a NMM model with independent mathematical and physical covers. The description of the Dirichlet boundaries and the method of assembling it into the equilib- rium equations may have a profound impact on the existence, uniqueness and stability of solutions. Moreover, the boundaries, for example, the free surface may divide some mathematical covers into different physical covers, leading to a discontinuity of hydraulic head and flux across the boundary. Traditionally, variational principle or the Galerkin method of weighted resid- uals is widely used to set up the equilibrium equations, mostly on the condition that the boundaries coincide with element vertices.

Our model is established according to energy-work seepage model and a concept model (i.e. pipe model) for constructing penalty function to deal with boundaries was first developed and presented in literature [38] in detail. In this approach, the model is established based on the work done by each component involved in the flow to establish the total potential energy based on the energy-work theorem. Meanwhile, the boundary cross-flow pipe model provides a method to uniformly consider the work done by flow across Dirichlet, Neumann and material boundaries. The total potential energy based on the energy-work theorem derived through this approach is (1) consistent with the variational principle related to domain and gravity flow with clearer physical meaning and (2) complete by including material boundaries and boundary conditions.

Specifically, for 2-D steady state flow simulation, the corresponding work components done by fluid gravity and flow in the porous media and across boundaries are as follows:

(1) the work corresponding to flow in the porous media:

$$W_s = \frac{1}{2}\gamma \iint \left( v_x \frac{\partial h}{\partial x} + v_y \frac{\partial h}{\partial y} \right) dxdy - \gamma \iint \frac{\partial v_y}{\partial} dxdydy \tag{17}$$

where $y$ is the vertical direction and the second-order time derivative of pressure is ignored.

(2) the work corresponding to fluid gravity:

$$W_g = \iint \gamma \, dydxdv_y = \gamma \iint \frac{\partial v_y}{\partial} dydxdy \tag{18}$$

(3) the work corresponding to Dirichlet boundary conditions:

$$W_{D} = \frac{1}{2}\gamma\zeta(h - h_0)^2 \tag{19}$$

where $\zeta$ is the linear coefficient of flux $q_i$ through each pipe versus hydraulic head difference $1'h_i$ between the two ends of each pipe, $h_0$ is the fixed hydraulic head at one pipe end in an assumed empty space and $h$ is the unknown hydraulic head at the other pipe end within the water flow domain to be solved [38].

(4) the work corresponding to material boundaries:

$$W_{m} = \frac{1}{2}\gamma\zeta(h_j - h_k)^2 \tag{20}$$

where $h_j$ and $h_k$ are hydraulic heads of two ends $j$ and $k$ of each pipe in different material media.

(5) the work corresponding to Neumann boundary conditions:

$$W_N = \gamma \iint \left( q_x \frac{\partial h}{\partial x} + q_y \frac{\partial h}{\partial y} \right) dxdy \tag{21}$$

where $(q_x, q_y)$ are the known flux projected to two directions of coordinate axis.

According to the energy-work theorem:

$$W_\phi + \Pi_\phi = 0 \tag{22}$$

where $\phi$ denotes work or energy component associated with domain flow, gravity, flow in pipes for Dirichlet boundaries, material boundaries or Neumann boundaries, respectively.

Combining Eqs. (17)–(22), we obtain the total potential energy $\Pi$ for a steady-state water flow as:

$$\Pi = \Pi_s + \Pi_g + \Pi_D + \Pi_m + \Pi_N \tag{23}$$

For cover $i$, equation $\frac{\partial IT}{\partial h_i} = 0$ represents the flux equilibrium on cover $i$:

$$\begin{pmatrix} C_{11} & C_{12} & C_{13} & \cdots & C_{1n} \\ C_{21} & C_{22} & C_{23} & \cdots & C_{2n} \\ C_{31} & C_{32} & C_{33} & \cdots & C_{3n} \\ \vdots & \vdots & \vdots & \ddots & \vdots \\ C_{n1} & C_{n2} & C_{n3} & \cdots & h_n \end{pmatrix} \begin{pmatrix} h_1 \\ h_2 \\ h_3 \\ \vdots \\ Q \end{pmatrix} = \begin{pmatrix} Q_1 \\ Q_2 \\ Q_3 \\ \vdots \\ \end{pmatrix} \tag{24}$$

where $h_i$ is the hydraulic head function of physical cover $i$ defined as Eq. (12), $C_{ij}$ is the component of the conductivity matrix, $Q_i$ is the flux term and $F$ is a constant. For higher order approximation, $h_i$ and $Q_i$ represent vectors with $m$ (the number of degrees of freedom of the physical cover $i$) components, and $C_{ij}$ represents a matrix with $m \times m$ components, respectively. For example, for Form 1 with linear physical cover hydraulic head distribution, each physical cover has three degrees of freedom. Therefore, $h_i$ and $Q_i$ are column vectors with three elements and $C_{ij}$ is a $3 \times 3$ matrix.

We can derive each component of $C_{ij}$ by

$$C_{ij} = \frac{\partial^2 IT}{\partial h_i \partial h_j} \tag{25}$$

and $Q_i$ by

$$Q_i = -\frac{\partial IT}{\partial h_i} \tag{26}$$

Based on simplex integration [43], the $C_{ij}$ and $Q_i$ contributed by each term in Eq. (23) are calculated, as listed in Appendix A.

### 2.4. Locating the free surface for free surface flow by second-order interpolation

For free surface flow, the schemes of locating and iterating the free surface are critically important. Because of the a priori unknown boundaries, such as FD and CD in Fig. 1, we need to assume the water flow domain for the first iteration (we consider no water flows above the free surface). In this study, we initially assume that the flow occupies the entire domain with a zero pressure boundary condition at the CE face. With this initial technique, we are able to avoid possible non-convergence caused by guessing a free surface if it is far from the real one. Thereafter, the final location is determined iteratively through a non-linear algorithm.

In the following sub-sections, we describe the method in more detail, including the description of the free surface nodes algorithm in the two forms of second-order approximation and iteration schemes to locate the free surface.

#### 2.4.1. Expressions and solutions for the free surface nodes in second-order NMM forms

(1) Form 1

The free surface nodes are located at the intersections of the free surfaces and elements, specifically at the edges of elements. Supposing one of the element edges consists of vertices $P_i(x_i, y_i)$ and $P_j(x_j, y_j)$. When using the first form of the second-order interpolation defined by Eqs. (13) and (14) for a free surface satisfying Eq. (6), we get the following expression for the free surface nodes:

$$\begin{cases} \sum_{m=1}^{3} (h_{m1} + h_{m2}x + h_{m3}y)(f_{m1} + f_{m2}x + f_{m3}y) = y \\ y = \frac{y_j - y_i}{x_j - x_i}(x - x_i) + y_i \\ (x - x_i)(x - x_j) + (y - y_i)(y - y_j) \le 0 \end{cases} \tag{27}$$

Equation set (27) contains a binary quadratic, which makes it difficult to solve directly.

Supposing a node $P_1(x_1, y_1)$ on an edge $P_iP_j$ with two ends $P_i(x_i, y_i)$ and $P_j(x_j, y_j)$, it satisfies the following expression:

$$\begin{cases} x_1 = (1 - \theta)x_i + \theta x_j \\ y_1 = (1 - \theta)y_i + \theta y_j \\ 0 \le \theta \le 1 \end{cases} \tag{28}$$

On the other hand, the hydraulic head of node $P_1$ on edge $P_iP_j$ is the weighted average of hydraulic heads at $P_i$ and at $P_j$. Based on the definition of weight function in Eq. (11) and its linear feature as in Eq. (13) shown in Fig. 4(b), we have:

$$h_1 = w_i h_i + w_j h_j$$

$$w_i = 1 - w_j = 1$$
$$\underline{\quad A}$$

(29)

$$w_i = 1 - w_j = 1$$
$$\underline{\quad A}$$

(29)

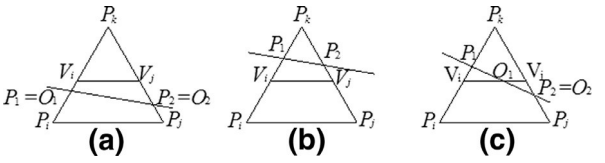


**Fig. 7.** Possible relative location of $P_1P_2$ and an element $P_iP_jV_jV_i$.

where $h_i$ and $h_j$ are the hydraulic heads at $P_i$ and $P_j$ respectively, computed by Eqs. (10), (13) and (14). If the edge $P_iP_j$ represents an edge of mathematical mesh, specifically $P_i$ and $P_j$ are the "stars" of physical covers $P_i$ and $P_j$ satisfying Eq. (14). The linear change of $h_i$ and $h_j$ on edge $P_iP_j$ can be simplified as:

$$\begin{cases} h_i = (1-\theta)(h_{i1} + h_{i2}x_i + h_{i3}y_i) + \theta\,(h_{i1} + h_{i2}x_j + h_{i3}y_j) \end{cases} \tag{30}$$

Substituting the parametric equation set (28), we obtain:

$$\begin{cases} x_1 = (1-\theta)x_i + \theta x_j \\ y_1 = (1-\theta)y_i + \theta y_j \\ h_1 = (1-\theta)(1-\theta)(h_{i1} + h_{i2}x_i + h_{i3}y_i) + \theta\,(h_{i1} + h_{i2}x_j + h_{i3}y_j) \\ \qquad + \theta\,(1-\theta)(h_{j1} + h_{j2}x_i + h_{j3}y_i) + \theta\,(h_{j1} + h_{j2}x_j + h_{j3}y_j) \\ h_1 = y_1 \\ 0 \le \theta \le 1 \end{cases} \tag{31}$$

Once $h_{mn}$ ($m = 1, 2, 3$ and $n = 1, 2, 3$) is solved, the Equation set (31) is a binary quadratic equation with the only unknown $\theta$. The real solution of $\theta$ is unique, limited by the last inequality. Solving $\theta$ and substituting it back, we get the solution for intersection $P_1(x_1, y_1)$. Repeating the same scheme, we can find the second intersection $P_2(x_2, y_2)$ of the free surface and triangle mesh edges. However, $P_1$ and $P_2$ are not always the free surface nodes $O_1$ and $O_2$, as shown in Fig. 7.

Supposing two of the element vertices are $V_i(x_{vi}, y_{vi})$ and $V_j(x_{vj}, y_{vj})$, the intersection of $P_1P_2$ and $V_iV_j$ is the real solution of $O_1$ or $O_2$, satisfying:

$$\begin{cases} x_0 = (1-\theta_1)x_1 + \theta_1 x_2 = (1-\theta_2)x_{Vi} + \theta_2 x_{Vj} \\ y_0 = (1-\theta_1)y_1 + \theta_1 y_2 = (1-\theta_2)y_{Vi} + \theta_2 y_{Vj} \\ 0 \le \theta_2 \le 1 \end{cases} \tag{32}$$

which provides the final solution for free surface nodes.

From Equation set (31), it is interesting to note that the normally used linear interpolation of two vertices for a free surface node is not applicable for second-order water flow analysis, due to the linear change of hydraulic head, as well as the linear change of the weight function on a physical cover. Take a 1-D model domain, for example, supposing the physical covers satisfy: $w_1 = 1 - y$, $h_1 = 1 + y$, $w_2 = y$, $h_2 = 2 - y$. Based on Eq. (10), the hydraulic head at any location is $h = 1 + 2y - 2y^2$. If the two ends of the model domain are located at $y_1 = \frac{1}{4}$ and $y_2 = \frac{3}{4}$. The hydraulic heads would be $h_1 = h_2 = \frac{11}{8}$. If interpolated linearly, the hydraulic head at any location within this model domain becomes $h = \frac{11}{8}$. It is obviously not correct.

(2) Form 2

In terms of the location of a point $P_1$ on an edge $P_iP_j$, the expression is the same as Eq. (28). As the weight functions are second-order, the hydraulic head of $P_1$ is represented by:

$$\begin{cases} h_1 = w_i h_i + w_o h_o + w_j h_j \\ w_i = 2/\theta - \frac{1}{2}(\theta - 1) \\ w_o = -4\theta(\theta - 1) \end{cases} \tag{33}$$

$$\left|\lfloor \quad \text{j} \quad = {}_{2}\theta\ /\theta - \underline{1}\right.$$

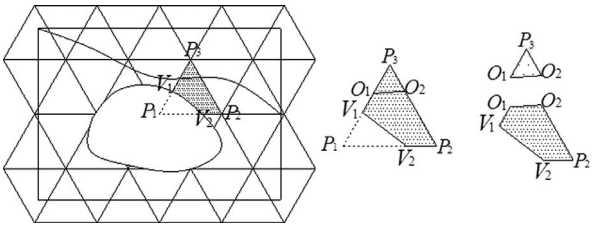


**Fig. 8.** Adjustment of elements across by phreatic surface.

where $i$ and $j$ denote two of the vertices of a triangle and $o$ denote a midpoint of a triangle mesh line. Since the hydraulic head is constant on a physical cover, $P_1$ can be solved by:

$$\begin{cases} x_1 = (1-\theta)x_i + \theta x_j \\ y_1 = (1-\theta)y_i + \theta y_j - 2\theta(\theta-1)h_o - 4\theta(\theta-\tfrac{1}{2})h_i - 2\theta(\theta-\tfrac{1}{2})h_j \\ h_1 = y_1 \\ 0 \le \theta \le 1 \end{cases} \tag{34}$$

Solving Eq. (34) and repeating Eq. (32), we obtain the real solution of free surface nodes.

*2.4.2. Iteration and convergence of locating the free surface*

During iterations, we approximate the free surface as a boundary dividing the entire domain into dry and wet parts. Across this boundary, there is no normal flux exchange between these two parts. Specifically, for example in Fig. 8 the free surface divides element $V_1V_2P_2P_3$ into two elements, $V_1V_2P_2O_2O_1$ (located in the wet part) and $O_1O_2P_3$ (in the dry part). Because there is no flux in element $O_1O_2P_3$, we directly reduce the integral area from $V_1V_2P_2P_3$ to $V_1V_2P_2O_2O_1$ to reduce the computational load. As for physical covers above $P_3$ (in the dry part), we still account for their contributions when establishing the conductivity matrix, in case that the simulated $O_1O_2$ is lower than the real free surface. At the same time, the boundary conditions are updated by removal of the pipes on the boundary above the release point (face EF) during successive iterations. After several iterations, the final free surface is constrained within a tolerance of $10^{-6}$ during two consecutive iterations. In the whole process, the mesh is only constructed once in pre-processing stage.

*2.5. Velocity and flux calculation*

*2.5.1. Velocity expression*

Once the freedoms $\{h_i(x, y)\}$ are calculated, the velocity function of an element is expressed as:

(1) Form 1

Combining Eqs. (2), (10), (13) and (14), we get the velocity function within an element expressed as:

$$\begin{bmatrix} v_x(x,y) \\ v_y(x,y) \end{bmatrix} = -\begin{bmatrix} k_{xx} & k_{xy} \\ k_{yx} & k_{yy} \end{bmatrix} \sum_{\substack{\lambda=i,j,k \\ \nu=1}} \begin{pmatrix} f_{\lambda 3\lambda 1}h_{\lambda 1} + f_{\lambda 3\lambda 2}h_{\lambda 2}x + w_{\lambda\lambda 3}h_{\lambda 2} + f_{\lambda 3\lambda 3}h_{\lambda 2}y \\ f_{\lambda 3\lambda 1}h_{\lambda 1} + f_{\lambda 3\lambda 2}h_{\lambda 2}x + w_{\lambda\lambda 3}h_{\lambda 2} + f_{\lambda 3\lambda 3}h_{\lambda 2}y \end{pmatrix} \tag{35}$$

(2) Form 2

Combining Eqs. (2), (10), (15) and (16), we get the velocity function within an element as:

$$\begin{bmatrix} v_x(x,y) \\ v_y(x,y) \end{bmatrix} = -\begin{bmatrix} k_{xx} & k_{xy} \\ k_{yx} & k_{yy} \end{bmatrix} \sum_{\lambda=1}^{6} \begin{pmatrix} \frac{\partial w_\lambda}{\partial x}h_\lambda \\ \frac{\partial w_\lambda}{\partial y}h_\lambda \end{pmatrix} \tag{36}$$

From Eqs. (35) and (36) we can see that the water velocity is linearly distributed, which is more capable to represent the local intensive change of hydraulic head, where there is a drainage tunnel.

*2.5.2. Flux into a drainage tunnel*

As shown in Fig. 9, we approximate a round tunnel by a hexadecagon, which intersects with mathematical lines to form elements such as elements 1, 2 and 3. The flux into a drainage tunnel is the velocity integrated on the tunnel edge expressed as:

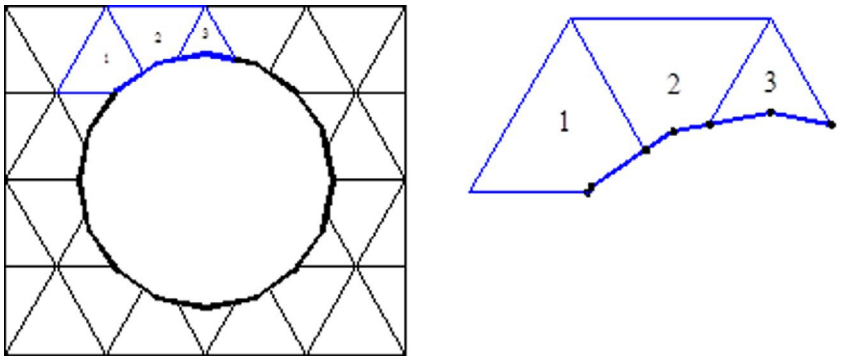


**Fig. 9.** Tunnel flux calculation model.

$$Q = \int_{f'} (v_x dy + v_y dx) \tag{37}$$

where $f'$ represents each straight line of a tunnel edge intersected by a mathematical line or another tunnel edge. Combining Eqs. (35) and (37) or Eqs. (36) and (37), we can see that the flux term is a second-order function of $x$ and $y$ on an edge. After being integrated and simplified, the flux through an edge $P_1P_2$ within one element is expressed as:

$$Q = \frac{1}{2}(v_{x1} + v_{x2})(y_2 - y_1) + \frac{1}{2}(v_{y1} + v_{y2})(x_2 - x_1) \tag{38}$$

where $v_{x1}$, $v_{y1}$ represent the velocities in $x$ and $y$ directions of vertex $P_1$, respectively and $v_{x2}$ and $v_{y2}$ represent those of vertex $P_2$. $v_{x1}$, $v_{x2}$, $v_{y1}$ and $v_{y2}$ are calculated by Eqs. (35) or (36). From $P_1$ to $P_2$, it is in the counterclockwise direction, which results flux directing towards the inner normal. From Eq. (38) we can obtain the linear change of velocity in both $x$ and $y$ directions on each edge.

## 3. *Demonstration examples*

On the basis of two forms of second-order approximation, the developed energy-work seepage model [38], the numerical techniques for locating the free surface and the calculation algorithm for flux into drainage tunnels, we developed a NMM model and a computer code for modeling free surface flow involving intense hydraulic head change. To demonstrate the accuracy and efficiency of the NMM model and the applicability of our code, we studied two examples: confined water flow into a drainage tunnel (Example 1) and free surface flow in a rectangular dam (Example 2). We compared our second-order results of flux with an existing analytical solution and linear solution for Example 1, and our free surface solution in Example 2 with our linear NMM solution and other numerical solutions from Oden and Kikuchi [28], Lacy and Prevost [29], Borja and Kishnani [32], Bardet and Tobita [35], in terms of meshing load, accuracy and convergence speed for these nonlinear water flow with inner intensive change problems.

### 3.1. Example 1: Flux into a drainage tunnel

In this example shown in Fig. 10, we calculated flux into an underground tunnel using the developed second-order NMM, and compared the result with the analytical solution by Lei [51] as well as the linear NMM result. The tunnel is located $H = 150$ m underground below the water table at the ground surface. The coefficient of permeability is $k_{xy}=k_{yx}=0$, $K=k_{xx}=k_{yy}=1 \times 10^{-8}$ m/s. The radius of the tunnel is $R = 10$ m. The analytical solution by Lei [51] is expressed as:

$$Q = \frac{2\pi KH}{\ln\left(H/R + \sqrt{H/R - 1}\right)} \tag{39}$$

$$h(x, y) = \frac{H}{\ln\left(H/R + \sqrt{H/R - 1}\right)} \ln \frac{x^2 + \left(y + \sqrt{H^2 - R^2}\right)^2}{x^2 + \left(y - \sqrt{H^2 - R^2}\right)^2} \tag{40}$$

Fig. 11 shows comparison of the simulation hydraulic head and velocity results using the second-order NMM with 1704 elements (2730 degrees of freedom) to those using the linear NMM with different numbers (5744, 6528 and 8730 elements with 2982, 3382, 4500 degrees of freedom, respectively). We further compared their calculated flux into the tunnel and simulated hydraulic head in an area of 20 m × 20 m around the tunnel and their maximum relative errors using the analytical solutions (as shown in Table 1). The second-order NMM produces accurate results with an error of 0.0234% for the flux into the tunnel and

4.318% for the hydraulic head. By contrast, the linear NMM with 8730 elements (over 5 times of the number of elements used in the second-order NMM) produces a flux error of 5.834% and a hydraulic head error of 7.213%.

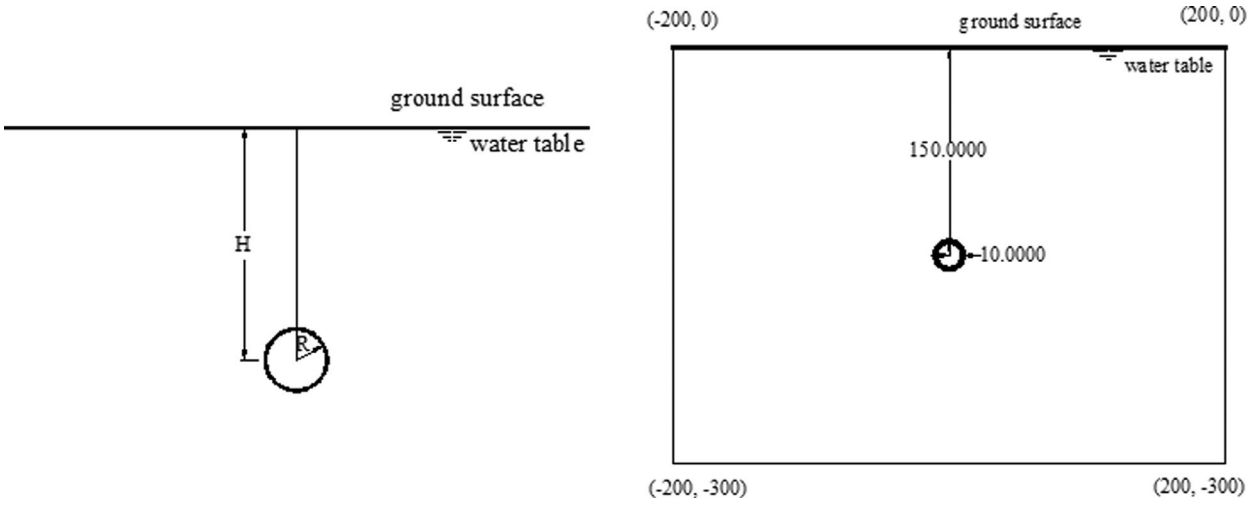


**Fig. 10.** Confined seepage into an underground drainage tunnel.

**Table 1**
Comparison of relative simulation errors of tunnel flux and hydraulic head using the second-order NMM and the linear NMM.

| | Number of elements | Number of degrees of freedom | Flux into the tunnel ($m^2/s$) | Relative error of flux | Maximum relative error of hydraulic head |
|---|---|---|---|---|---|
| **Linear NMM** | 5744 | 2982 | $2.15391 \times 10^{-6}$ | −0.22256 | −0.07011 |
| **Linear NMM** | 6528 | 3382 | $2.51043 \times 10^{-6}$ | −0.09388 | −0.0636 |
| **Linear NMM** | 8730 | 4500 | $2.6089 \times 10^{-6}$ | −0.05834 | −0.07213 |
| **Second-order NMM** | **1704** | **2730** | $\mathbf{2.77117 \times 10^{-6}}$ | **0.000234** | **−0.04318** |
| **Analytical [51]** | | | $2.77052 \times 10^{-6}$ | | |

**Table 2**
Comparison of simulation parameters for various simulation methods.

| | Number of elements | Number of iteration | Tolerance | SOR factor |
|---|---|---|---|---|
| **Oden and Kikuchi [28]** | 200 | 20 | — | 1.7 |
| **Lacy and Prevost [29]** | 200 | 11 | 0.001 | — |
| **Bardet and Tobita [35]** | 200 | 135 | 0.0001 | 1.2 |
| **Borja and Kishnani [32]** | 200 | 4 | $10^{-10}$ | — |
| **Linear NMM [38]** | 236 | 13 | $10^{-6}$ | (1.0, 2.0) |
| **Second-order NMM** | **56** | **4** | $\mathbf{10^{-6}}$ | **(1.0, 2.0)** |

From this example we can see that the second-order NMM can accurately simulate the local, large change in hydraulic head around tunnels, and accurately calculate the flux of the drainage tunnels with a coarse, fixed mesh, indicating promising application to projects involving flux prediction.

### *3.2. Example 2: A homogeneous rectangular dam with tail water*

Example 2 involves free surface flow through a homogeneous rectangular dam driven by the head difference between 10 m at the upstream face and 2 m at the downstream face (Fig. 12). Fig. 12(a) shows the final hydraulic head distribution in the whole model domain, whereas Fig. 12(b) shows the results of free surface with iterations. The results show that for the second- order approximation, convergence within a tolerance of $10^{-6}$ is reached in only 4 iterations. Fig. 12(c) presents a comparison of the free-surface profile simulated by the second-order NMM to those of the linear NMM [38] and other numerical solu- tions in the literature (using Finite Element Method by Lacy and Prevost [29], Oden and Kikuchi [28] and Borja and Kishnani [32]; and Finite Difference Method by Bardet and Tobita [35]). The comparison shows that our second-

order NMM profile is close to that by Lacy and Prevost [29], with a maximum difference of 3.08% for free surface nodes and 1.34% for the release point.

Table 2 lists model parameters and number of iterations required for convergence for all the solutions. In our simulation, we use a Successive Over-Relaxation (SOR) algorithm to solve the equilibrium equations. We found that the change of SOR factor

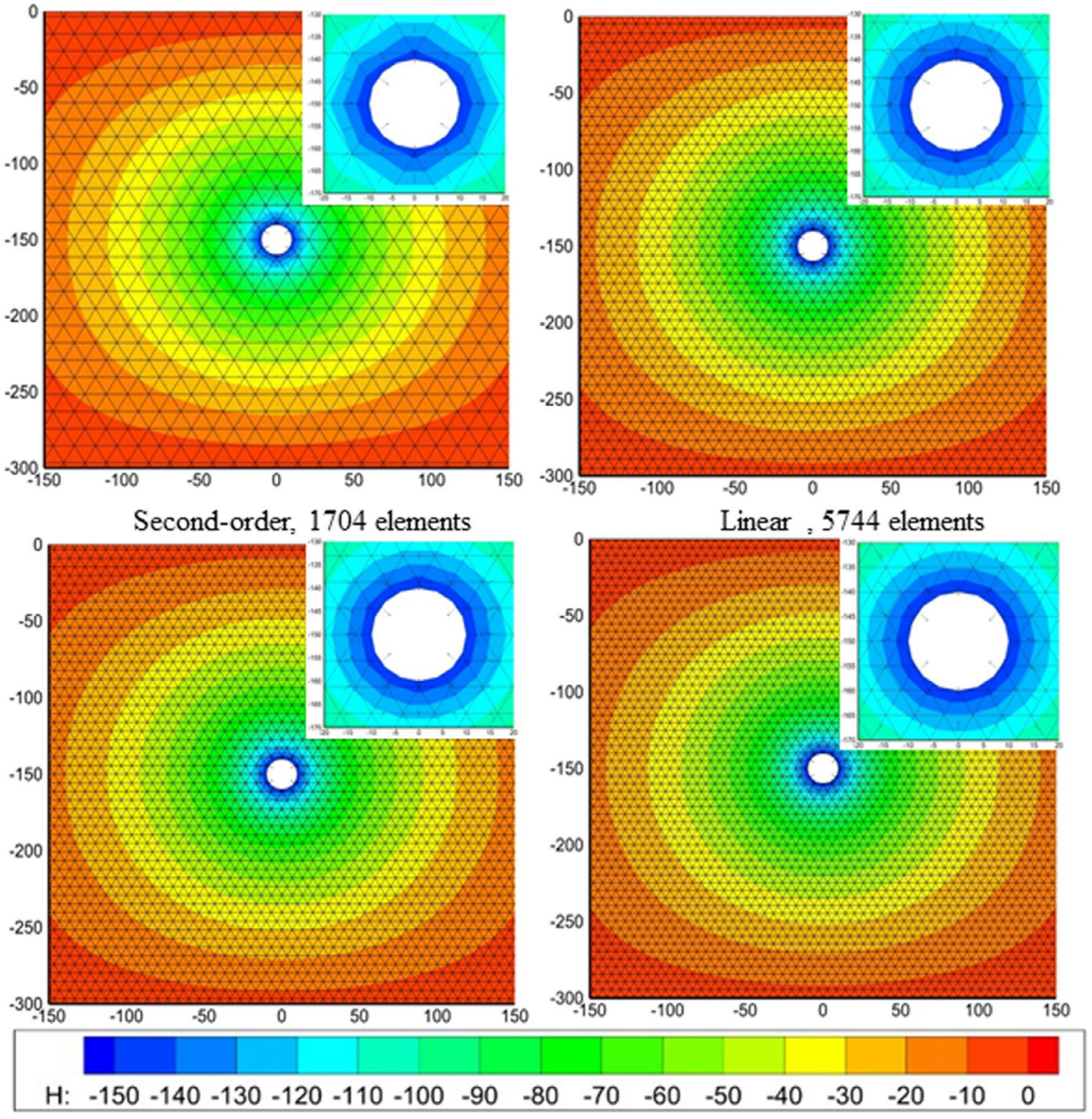


**Fig. 11.** Comparison of the hydraulic head and velocity fields simulated using the second-order NMM with 1704 elements and using the linear NMM with 5744, 6528, and 8730 elements.

within (1.0, 2.0) has a small impact on the convergence speed. From this example we see that the second-order NMM model developed in this study achieve a rapid convergence within a stringent tolerance even with a relatively coarse mesh.

## 4. An application: a sloped earth dam with an inner drainage tunnel

This is an application about free surface flow through a sloped earth dam with a hydraulic head of 110 m on the vertical upstream surface and 70 m on the slanted downstream surface (as shown in Fig. 13a). A drainage tunnel is centered at (70, 55) m inside the dam. The coefficient of permeability is $1 \times 10^{-7}$ m/s. The boundary of the tunnel satisfies the condition of zero pressure, i.e., expressed as in Eq. (4) where $H_i$ is the elevation. Fig. 13 shows the solution convergence with iterations using the linear NMM and the second-order NMM with 872 elements. It takes 17 iterations for the linear NMM and only 4 iterations for the second-order NMM to converge with the tolerance is $10^{-6}$ (if we set larger tolerance, the difference of the iterations required is much smaller).

The convergence of hydraulic head is far from the convergence of velocity in the field, the latter requires more computational load with longer time. Fig. 14 (a) and (b) show the final steady-state head distribution using the linear NMM with 5550 elements

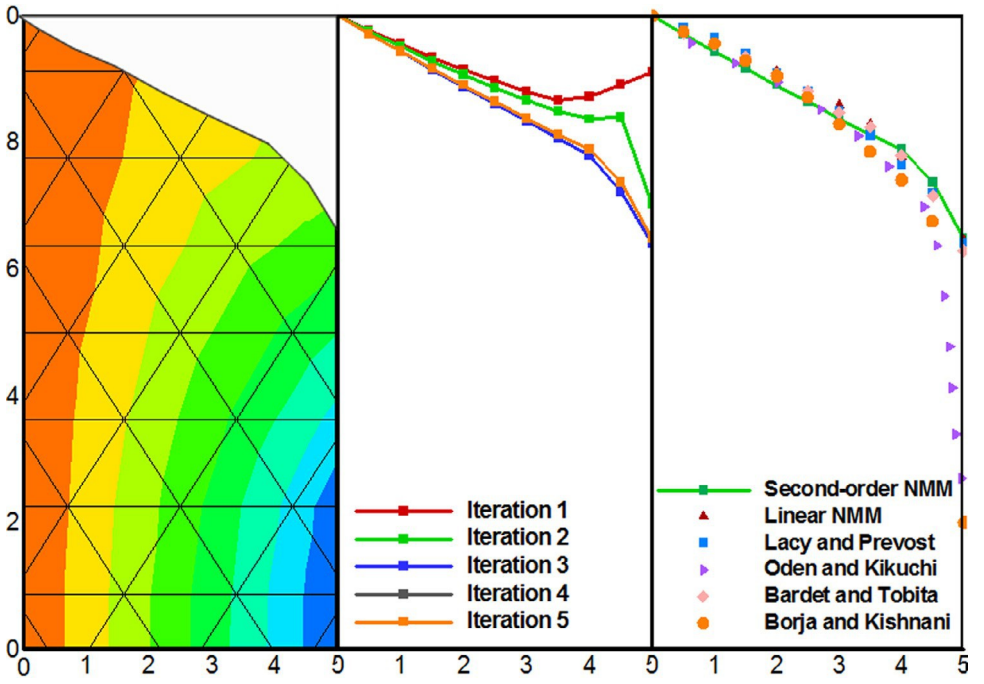


**Fig. 12.** Simulation results of the second-order NMM with 8 layers and 56 elements: (a) contour of hydraulic head in the whole domain, (b) profiles of the phreatic surface with iterations, and (c) comparison of the final phreatic surface profile with those of numerical solutions available in the literature.

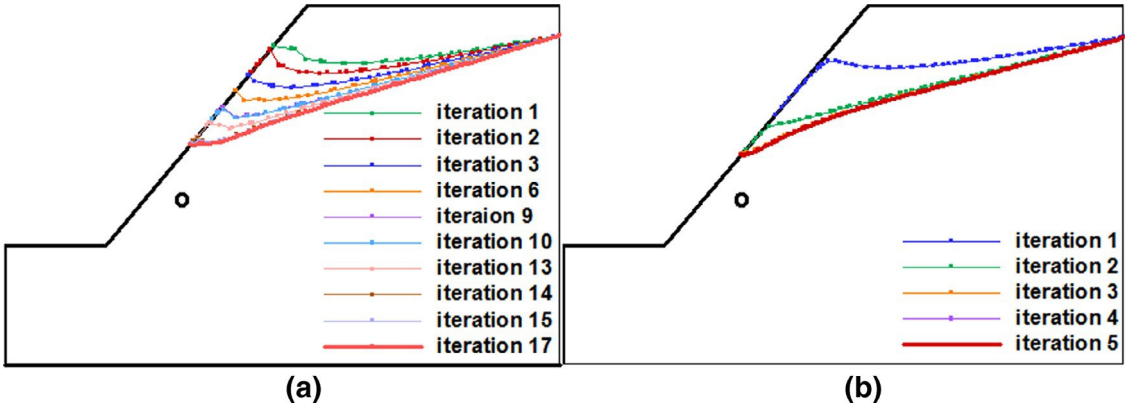


**Fig. 13.** Comparison of simulation convergence for unconfined seepage through a dam with slanted downstream face and an inner drainage tunnel: (a) 17 iterations with the linear NMM and (b) 5 iterations with the second-order NMM with tolerance of $10^{-6}$.

and second-order NMM with 2469 elements, respectively. The flux calculated by the second-order NMM is $3.183 \times 10^{-6}$ m$^2$/s and that by the first-order NMM is $3.092 \times 10^{-6}$ m$^2$/s.

Note that it is an example with a relatively small tunnel in a computation domain, which involves very strong local change around the tunnel. For such a case, it is possible to consider and design a series of tunnels with certain spacing. If the size of the tunnel is increased, the required mesh load could be reduced.

## 5. Discussion

In this study, we developed a new second-order NMM model for analysis of free surface flow possibly with inner drains and tested it on application examples that were designed for verification. From those examples, we showed that the method can accurately and efficiently model this nonlinear, moving- boundary problem, possibly involving high local gradient with fixed mathematical mesh. The model and scheme developed in this study can easily be extended to transient flow analysis. For transient flow modeling, initial conditions and changing boundary conditions could be implemented directly into the code. The transient mass changes are related to aquifer compression and free surface changes with time. With proper time-marching algorithm, it is straightforward to transform the aquifer compression to both the conductivity and flux terms according to

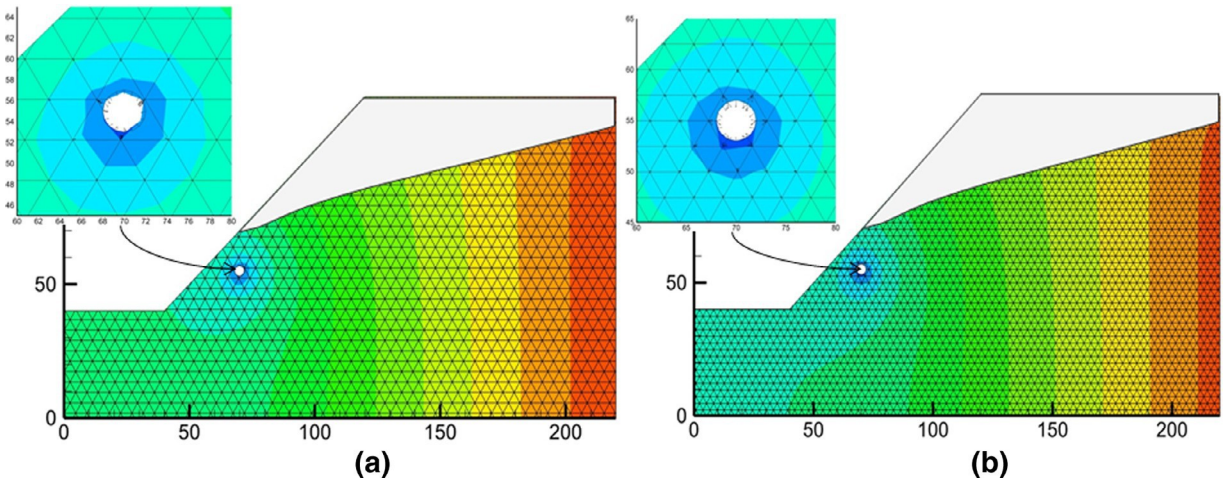


**Fig. 14.** Simulation results of hydraulic head distribution and velocity using (a) the second-order NMM with 2469 elements and (b) the linear NMM with 5550 elements.

energy- work model. For changes in the free surface with time, the scheme developed in this study for steady-state could be used to locate the free surface at the initial step. Afterwards, we could solve the free surface location for each time step by implicitly regarding the transient free surface changes as a flux boundary.

This model could be extended for three-dimensional analysis from its current two-dimensional form. The meshing will be very efficient as we use uniform simplex to form the fixed mathematical mesh. The algorithms for calculating the free surface will be similar as for two-dimensional analysis developed in this work. Moreover, the cover-based NMM will be very flexible for choosing different approximation orders in different directions. For example, for free surface low analysis, we may focus more on the vertical dimension than on the horizontal dimensions. Then we can increase the order in the vertical dimension only, with the usage of triangular prism to form fixed mathematical mesh.

The developed model for free surface flow analysis could be a future key component of coupled hydro-mechanical analyses. As a fixed-mesh model, the method is suitable for modeling hydro-mechanical behavior, encompassing both continuous and discontinuous processes. In addition, it inherits the aforementioned advantages for flow modeling, as well as the advantages of NMM, in terms of: (1) the fixed mathematical mesh, avoiding expensive computational efforts in meshing; (2) accurate integra- tion on arbitrary shape of elements using simplex integration; and (3) flexibly enhanced approximation precision.

## 6. Conclusions

In order to accurately and efficiently solve the nonlinear problem of flow with the free surface priori unknown and the difficulty of modeling drains which could dramatically increase the meshing load, in this study we developed a second-order NMM model, including:

(1) two forms of second-order approximation with triangles forming mathematical covers. In the first form, we increased the function on each physical cover from constant to linear functions. In the second form, we increase the order of weight functions by increasing the number of covers of an overlapped element;
(2) a complete and rigorous potential energy expression, in which each term can be related to a process with clear physical meaning based on the energy-work seepage model. Together with our proposed pipe model for constructing penalty function, we could uniformly deal with Dirichlet, Neumann and material boundaries, which are not required to coincide with element vertices;
(3) solution of free surface nodes in two forms of second-order approximation. We transformed the binary quadratic equation set to a quadratic equation, by making full use of the features of weight functions and physical cover functions defined in NMM;
(4) an efficient iteration scheme for the free surface with no need to re-mesh by fixing the mathematical covers and updating the physical covers crossed by free surface;
(5) expression of velocity and flux by second-order approximation. The velocity, the first derivative of hydraulic head has linear distribution within an element, enabling to reduce mesh load dramatically to represent local intensive changes. The flux, the integration of velocity, inherits the advantage of velocity by second-order approximation.

Finally, we demonstrate our methodology and NMM code by comparing our second-order results confined or free surface flow models with drainage tunnels with linear NMM, analytical or other available numerical simulation results. We show that (1) the two forms of second-order approximation yield consistent results even for modeling examples involving water flow with a priori-unknown free surface and problems involving local intensive change with inner drains. (2) The results of the second-order

NMM with coarse numerical mesh was comparable with those of other methods in terms of accuracy, thus at a high convergence speed, demonstrating an excellent numerical efficiency. Furthermore, this model will be naturally extended to transient analysis in three-dimensional space and will be a key part of analysis of coupled hydro-mechanical processes with moving boundaries in continuous and discontinuous geological media.

**Acknowledgments**

The research was supported by the National Natural Science Foundation (No. 51179060) and the Education Ministry Foundation of China (No. 20110094130002), the Fundamental Research Funds for the Central Universities (No. 2015B05114), Graduates Science Innovation Research Project of Jiangsu Province (No. CXZZ12_0230), China Scholarship Council and in part, supported by the Program for Changjiang Scholars and Innovative Research Team in University (No. IRT1125), the 111 Project (No. B13024) and by the U.S. Department of Energy to Lawrence Berkeley National Laboratory under contract No. DE-AC02-05CH11231.

**Appendix A**

Values of $C_{ij}$ and $Q_i$ in equilibrium equations based on second-order interpolation

*A1. Values by second-order interpolation in Form 1*

(1) $C_{ij}$ corresponding to domain flow and gravity

$$C_{ij}(1,1) = \quad + \quad + \; {}_{i3}S$$

$$C_{ij}(1,2) = \quad + \quad + \quad + \quad + + \quad + \quad + \; f_{j3}S_y$$

$$C_{ij}(1,3) = \quad + \quad + \quad + \quad + + \quad + \quad + \; ) f_{i3}S_x$$

$$C_{ij}(2,2) = \quad + \quad + \quad + \quad + \quad + \quad + \quad r \quad r \quad (2k_{xx} f_{j2} + k_{xy} f$$

$$_{j3}) f_{i3} S_{xy} C_{ij}(2,3) = \quad + \quad + \quad + \quad + \quad + \quad + \quad + \quad k_{\quad} f_{\quad} + 2k_{\quad} f_{\quad}) f_{i3}S_{yy} + (2k_{xy} f_{i2} f_{j1} + k_{yy}$$

$$f_{i3} f_{j1} + k_y + \quad + \quad + \quad + \quad + \quad + \quad + \quad + \quad$$

$$C_{ij}(3,3) = \quad + \quad + \quad + \quad + \quad + \quad + \quad r \quad r \quad k_{yx} f_{i2} + 2k_{yy} f_{i3}) f$$

$$_{j2}$$

(2) $C_{ij}$ and $Q_i$ corresponding to Dirichlet boundary conditions

$$C_{ij}(1,1) = \zeta w_i(x_0, y_0) w_j(x_0, y_0)$$
$$C_{ij}(1,2) = \zeta w_i(x_0, y_0) w_j(x_0, y_0) x_0$$
$$C_{ij}(1,3) = \zeta w_i(x_0, y_0) w_j(x_0, y_0) y_0$$
$$C_{ij}(2,2) = \zeta w_i(x_0, y_0) w_j(x_0, y_0) x^2{}_0$$
$$C_{ij}(2,3) = \zeta w_i(x_0, y_0) w_j(x_0, y_0) x_0 y_0$$
$$C_{ij}(3,3) = \zeta w_i(x_0, y_0) w_j(x_0, y_0) y^2{}_0$$
$$Q_{i1} = \zeta w_i(x_0, y_0) h_0$$
$$Q_{i2} = \zeta w_i(x_0, y_0) h_0 x_0$$
$$Q_{i3} = \zeta w_i(x_0, y_0) h_0 y_0$$

(3) $C_{ij}$ corresponding to material boundaries

$$C_{ij}(1,1) = \zeta w_i(x_1, y_1) w_j(x_1, y_1) \quad C_{i\,j}(1,1) = \zeta w_{\,i}(x_2, y_2) w_{\,j}(x_2, y_2)$$
$$C_{ij}(1,2) = \zeta w_i(x_1, y_1) w_j(x_1, y_1) x_1 \quad C_{i\,j}(1,2) = \zeta w_{\,i}(x_2, y_2) w_{\,j}(x_2, y_2) x_2$$
$$C_{ij}(1,3) = \zeta w_i(x_1, y_1) w_j(x_1, y_1) y_1 \quad C_{i\,j}(1,3) = \zeta w_{\,i}(x_2, y_2) w_{\,j}(x_2, y_2) y_2$$
$$C_{ij}(2,2) = \zeta w_i(x_1, y_1) w_j(x_1, y_1) x^2{}_1 \quad C_{i\,j}(2,2) = \zeta w_{\,i}(x_2, y_2) w_{\,j}(x_2, y_2) x^2{}_2$$
$$C_{ij}(2,3) = \zeta w_i(x_1, y_1) w_j(x_1, y_1) x_1 y_1 \quad C_{i\,j}(2,3) = \zeta w_{\,i}(x_2, y_2) w_{\,j}(x_2, y_2) x_2 y_2$$
$$C_{ij}(3,3) = \zeta w_i(x_1, y_1) w_j(x_1, y_1) y^2{}_1 \quad C_{i\,j}(3,3) = \zeta w_{\,i}(x_2, y_2) w_{\,j}(x_2, y_2) y^2{}_2$$
$$C_{ij}(1,1) = -\zeta w_i(x_1, y_1) w_{\,j}(x_2, y_2) \quad C_{i\,j}(1,1) = -\zeta w_{\,i}(x_2, y_2) w_j(x_1, y_1)$$

$C_{ij}(1, 2) = -\zeta\, w_i(x_1, y_1) w_j(x_2, y_2) x_2\; C_{ij}(1, 2) = -\zeta\, w_i(x_2, y_2) w_j(x_1, y_1) x_1\; C_{ij}(1, 3) = -\zeta\, w_i(x_1, y_1) w_j(x_2, y_2) y_2\; C_{ij}(1, 3) = -\zeta\, w_i(x_2, y_2) w_j(x_1, y_1) y_1$

$$C_{ij}(2,2) = -\zeta\, w_i(x_1, y_1) w_j(x_2, y_2) x_1 x_2 \quad C_{ij}(2,2) = -\zeta\, w_i(x_2, y_2) w_j(x_1, y_1) x_1 x_2$$
$$C_{ij}(2,3) = -\zeta\, w_i(x_1, y_1) w_j(x_2, y_2) x_1 y_2 \quad C_{ij}(2,3) = -\zeta\, w_i(x_2, y_2) w_j(x_1, y_1) y_1 x_2$$
$$C_{ij}(3,3) = -\zeta\, w_i(x_1, y_1) w_j(x_2, y_2) y_1 y_2 \quad C_{ij}(3,3) = -\zeta\, w_i(x_2, y_2) w_j(x_1, y_1) y_1 y_2$$

(4) $Q_i$ corresponding to Neumann boundary conditions

$$Q_{i1} = S(q_x f_{i2} + q_y f_{i3})$$
$$Q_{i2} = q_x f_{i1} S + (2q_x f_{i2} + q_y f_{i3}) S_x + q_x f_{i3} S_y$$
$$Q_{i3} = q_y f_{i1} S + q_y f_{i3} S_x + (q_x f_{i2} + 2q_y f_{i3}) S_y$$

*A2. Values by second-order interpolation in Form 2*

(1) $C_{ij}$ corresponding to domain flow and gravity

$$C_{ij} = \int \Big[ (k_{xx} f_{i2} + k_{yx} f_{i3}) f_{j2} + (k_{xy} f_{i2} + k_{yy} f_{i3}) f_{j3} \Big] S$$
$$+ \int \Big[ 2k_{xx}(f_{i4} f_{j2} + f_{i2} f_{j4}) + 2(k_{xy} f_{i3} f_{j4} + k_{yx} f_{i4} f_{j3}) + (k_{xy} f_{i2} f_{j5} + k_{yx} f_{i5} f_{j2}) + k_{yy}(f_{i5} f_{j3} + f_{i3} f_{j5}) \Big] S_x$$
$$+ \int \Big[ k_{xx}(f_{i5} f_{j2} + f_{i2} f_{j5}) + 2(k_{xy} f_{i2} f_{j6} + k_{yx} f_{i6} f_{j2}) + (k_{xy} f_{i5} f_{j3} + k_{yx} f_{i3} f_{j5}) + 2k_{yy}(f_{i6} f_{j3} + f_{i3} f_{j6}) \Big] S_y$$
$$+ \int \Big[ 2(2k_{xx} f_{i4} + k_{yx} f_{i5}) f_{j4} + (2k_{xy} f_{i4} + k_{yy} f_{i5}) f_{j5} \Big] S_{xx}$$
$$+ \int \Big[ (k_{xx} f_{i5} + 2k_{yx} f_{i6}) f_{j5} + 2(k_{xy} f_{i5} + 2k_{yy} f_{i6}) f_{j6} \Big] S_{yy}$$
$$+ \int \Big[ 2k_{xx}(f_{i4} f_{j5} + f_{i5} f_{j4}) + (k_{xy} + k_{yx}) f_{i5} f_{j5} + 4(k_{xy} f_{i4} f_{j6} + k_{yx} f_{i6} f_{j4}) + 2k_{yy}(f_{i5} f_{j6} + f_{i6} f_{j5}) \Big] S_{xy}$$

(2) $C_{ij}$ and $Q_i$ corresponding to Dirichlet boundary conditions

$$C_{ij} = \zeta w_i(x_0, y_0) w_j(x_0, y_0)$$
$$Q_i = \zeta w_i(x_0, y_0) h_0$$

(3) $C_{ij}$ corresponding to material boundaries:

$$C_{ij} = \zeta w_i(x_1, y_1) w_j(x_1, y_1) \quad C_{ij} = -\zeta\, w_i(x_1, y_1) w_j(x_2, y_2)$$
$$C_{ij} = -\zeta\, w_i(x_2, y_2) w_j(x_1, y_1) \quad C_{ij} = \zeta w_i(x_2, y_2) w_j(x_2, y_2)$$

(4) $Q_i$ corresponding to Neumann boundary conditions

$$Q_i = S(f_{i2} q_x + f_{i3} q_y) + (2 f_{i4} q_x + f_{i5} q_y) S_x + (f_{i5} q_x + 2 f_{i6} q_y) S_y$$

## References


[1] J. Bear, Dynamics of Fluids in Porous Media, American Elsevier Publishing Company, New York, 1972.
[2] J. Bear, Hydraulics of Groundwater, McGraw-Hill, New York, 1979.
[3] V. Bedekar, R.G. Niswonger, K. Kipp, S. Panday, M. Tonkin, Approaches to the simulation of unconfined flow and perched groundwater flow, Gr. Water 50 (2) (2012) 187–198.
[4] S.P. Neuman, P.A. Witherspoon, Finite element method of analyzing steady seepage with a free surface, Water Resour. Res. 6 (3) (1970) 889–897.
[5] T. Chisyaki, A study on confined flow of ground water through a tunnel, Gr. Water 22 (2) (1984) 162–167.
[6] D. Meiri, Unconfined groundwater flow calculation into a tunnel, J. Hydrol. 82 (1) (1985) 69–75.
[7] M. Foster, R. Fell, M. Spannagle, The statistics of embankment dam failures and accidents, Can. Geotech. J. 37 (5) (2000) 1000–1024.
[8] M. Foster, R. Fell, M. Spannagle, A method for assessing the relative likelihood of failure of embankment dams by piping, Can. Geotech. J. 37 (5) (2000) 1025–1061.
[9] T.K. Huang, Stability analysis of an earth dam under steady state seepage, Comput. Struct. 58 (6) (1996) 1075–1082.
[10] R.A. Freeze, Three-Dimensional, Transient, Saturated-Unsaturated Flow in a Groundwater Basin, Water Resour. Res. 7 (1971) 347–366.
[11] P.S. Huyakorn, E.P. Springer, V. Guvanasen, T.D. Wadsworth, A three-dimensional finite-element model for simulating water flow in variably saturated porous media, Water Resour. Res. 22 (1986) 1790–1808.
[12] J.H. Zhang, Q.J. Xu, Z.Y. Chen, Seepage analysis based on the unified unsaturated soil theory, Mech. Res. Commun. 28 (2001) 107–112.
[13] O.C. Zienkiewicz, A.H.C. Chan, M. Pastor, B.A. Schrefler, T. Shiomi, Computational Geomechanics with Special Reference to Earthquake Engineering, John Wiley & Sons, 1999.
[14] K.A. Pericleous, G.J. Moran, S.M. Bounds, P. Chow, M. Cross, Three-dimensional free surface modelling in an unstructured mesh environment for metal processing applications, Appl.Math. Model. 22 (1998) 895–906.
[15] H. Saghi, M.J. Ketabdari, M. Zamirian, A novel algorithm based on parameterization method for calculation of curvature of the free surface flows, Appl. Math. Model. 37 (2013) 570–585.
[16] X.F. Yang, S.L. Peng, M.B. Liu, A new kernel function for SPH with applications to free surface flows, Appl. Math. Model. 38 (2014) 3822–3833.
[17] V.T. Nguyen, 3D Numerical simulation of free surface flows over hydraulic structures in natural channels and rivers, Appl. Math. Model. (2015) http://dx.doi.org/10.1016/j.apm.2015.01.046 .
[18] C.W. Cryer, On the approximate solution of free boundary problems using finite differences, J. Association Comput. Mach. 17 (3) (1970) 397–411.
[19] G. Gioda, C. Gentile, A nonlinear programming analysis of unconfined steady-state seepage, Int. J. Numer. Anal. Methods Geomech. 11 (1987) 283–305.
[20] A. Ouria, M.M. Toufigh, Application of Nelder-Mead simplex method for unconfined seepage problems, Appl. Math. Model. 33 (2009) 3589–3598.
[21] A.K. Chugh, H.T. Falvey, Seepage analysis in a zoned anisotropic medium by the boundary element method, Int. J. Numer. Anal. Methods Geomech. 8 (1984) 399–407.
[22] M. Darbandi, S.O. Torabi, M. Saadat, Y. Daghighi, D. Jarrahbashi, A moving-mesh finite-volume method to solve free-surface seepage problem in arbitrary geometries, Int. J. Numer. Anal. Methods Geomech. 31 (2007) 1609–1629.

[23] E. Bresciani, J.R. Dreuzy, A finite volume approach with local adaptation scheme for the simulation of free surface flow in porous media, Int. J. Numer. Anal. Methods Geomech. 36 (2012) 1574–1591.
[24] S. Shahrokhabadi, M.M. Toufigh, The solution of unconfined seepage problem using Natural Element Method (NEM) coupled with Genetic Algorithm (GA), Appl. Math. Model. 37 (2013) 2775–2786.
[25] C.S. Desai, Finite element residual schemes for unconfined flow, Int. J. Numer. Methods Eng. 10 (1976) 1415–1418.
[26] C.S. Desai, G.C. Li, Residual flow procedure and application for free surface flow in porous media, Adv. Water Resour. 6 (1983) 27–35.
[27] Y. Wang, The modified initial flow method for 3-D unconfined seepage computation, J. Hydraul. Eng. (3) (1998) 68–73.
[28] J.T. Oden, N. Kikuchi, Recent advances: theory of variational inequalities with applications to problems of flow through porous media, Int. J. Eng. Sci. 18 (1980) 1173–1284.
[29] S.J. Lacy, J.H. Prevost, Flow through porous media: a procedure for locating the free surface, Int. J. Numer. Anal. Methods Geomech. 11 (1987) 585–601.
[30] H. Zheng, H.C. Dai, D.F. Liu, A variational inequality formulation for unconfined seepage problems in porous media, Appl. Math. Model. 33 (2009) 437–450.
[31] K.J. Bathe, M.R. Khoshgoftaar, Finite element free surface seepage analysis without mesh iteration, Int. J. Numer. Anal. Methods Geomech. 3 (1979) 13–22.
[32] R.I. Borja, S.S. Kishnani, On the solution of elliptic free boundary problems via Newton's method, Comput. Methods Appl. Mech. Eng. 88 (1991) 341–361.
[33] M.J.K. Parsi, F. Daneshmand, Unconfined seepage analysis in earth dams using smoothed fixed grid finite element method, Int. J. Numer. Anal. Methods Geomech. 36 (2012) 780–797.
[34] M.H. Bazyar, A. Graili, A practical and efficient numerical scheme for the analysis of steady state unconfined seepage flow, Int. J. Numer. Anal. Methods Geomech. 36 (2012) 1793–1812.
[35] J.P. Bardet, T. Tobita, A practical method for solving free-surface seepage problems, Comput. Geotech. 29 (2002) 451–475.
[36] G.X. Li, J.H. Ge, Y.X. Jie, Free surface seepage analysis based on the element-free method, Mech. Res. Commun. 30 (2003) 9–19.
[37] Y. Ohnishi, M. Tanaka, T. Koyama, K. Mutoh, Manifold method in saturated-unsaturated unsteady groundwater flow analysis, in: B. Amadei (Ed.), Third International Conference on Analysis of Discontinuous Deformation—From theory to practice, Vail, Colorado, 3 – 4, January 1999, pp. 221–230.
[38] Y. Wang, M.S. Hu, Q.L. Zhou, J. Rutqvist, Energy-work-based numerical manifold seepage analysis with an efficient scheme to locate the phreatic surface, Int. J. Numer. Anal. Methods Geomech. 38 (15) (2014) 1633–1650.
[39] H. Zheng, F. Liu, C.G. Li, Primal mixed solution to unconfined seepage flow in porous media with numerical manifold method, Appl. Math. Model. 39 (2015) 794–808.
[40] G. Fipps, R.W. Skaggs, J.L. Nieber, Drains as a boundary condition in finite elements, Water Resour. Res. 22 (11) (1986) 689–707.
[41] S.H. Chen, L.L. Xue, G.S. Xu, I. Shahrour, Composite element method for the seepage analysis of rock masses containing fractures and drainage holes, Int. J. Rock Mech. Min. Sci 47 (5) (2010) 762–770.
[42] G.H. Shi, Manifold method of material analysis, in: Transaction of the 9th Army Conference on Applied Mathematics and Computing, 18-21 June, Minneapolis, Army Mathematics Steering Committee, 1991, pp. 57–76.
[43] G.H. Shi, Simplex Integration for Manifold Method, FEM and DDA. Discontinuous Deformation Analysis (DDA) and Simulations of Discontinuous Media, TSI press, 1996, pp. 205–262.
[44] G.H. Shi, R.E. Goodman, Two dimensional discontinuous deformation analysis, Int. J. Numer. Anal. Methods Geomech. 9 (6) (1985) 541–556.
[45] G.W. Ma, X.M. An, L. He, The numerical manifold method: a review, Int. J. Comput. Methods 7 (1) (2010) 1–32.
[46] L. He, Three Dimensional Numerical Manifold Method and Rock Engineering Applications, Nanyang Technological University, 2011 PhD Dissertation.
[47] M. Hu, Y. Wang, J. Rutqvist, On continuous and discontinuous approaches for modeling groundwater flow in heterogeneous media using the Numerical Manifold Method: Model development and comparison, Adv. Water Resour. 80 (2015) 17–29.
[48] P. Solin, K. Segeth, I. Dolezel, Higher-Order Finite Element Methods, Chapman & Hall/CRC Press, 2003.
[49] G.Q. Chen, Y. Ohnishi, T. Ito, Development of High-order Manifold Method, Int. J. Numer. Methods Eng. 43 (1998) 685–712.
[50] G.X. Zhang, Y. Sugiura, H. Hasegawa, G.L. Wang, The second order manifold method with six node triangle mesh, Struct. Eng./Earthq. Eng. 19 (1) (2002) 1–9.
[51] S. Lei, An analytical solution for steady flow into a tunnel, Gr. Water 37 (1) (1999) 23–26.